Single-mode photonic crystal nanobeam lasers monolithically grown on Si for dense integration

Taojie Zhou, Mingchu Tang, *Member, IEEE*, Haochuan Li, Zhan Zhang, Yuzhou Cui, Jae-seong Park, Markel Martin, Thierry Baron, Siming Chen, *Senior Member, IEEE*, Huiyun Liu, and Zhaoyu Zhang

***Abstract*—Ultra-compact III-V nanolasers monolithically integrated on Si with ultra-low energy consumption and small modal volume have been emerged as one of the most promising candidates to achieve Si on-chip light sources. However, the significant material dissimilarities between III-V and Si fundamentally limit the performance of Si-based III-V nanolasers. In this work, we report 1.3 μm InAs/GaAs quantum-dot photonic-crystal (PhC) nanobeam lasers directly grown on complementary metal-oxide-semiconductor compatible on-axis Si (001) substrates. The continuous-wave optically pumped PhC nanobeam lasers exhibited a single-mode operation, with an ultra-low lasing threshold of ~ 0.8 μW at room temperature. In addition, a nanoscale physical volume of ~ 8 × 0.53 × 0.36 μm^3 (~ 25 $(\lambda n^{-1})^3$) was realized through a small number of air-holes in PhC nanobeam laser. The promising characteristics of the PhC nanobeam lasers with small footprint and ultra-low energy consumption show their advanced potential towards densely integrated Si photonic integrated circuits.**

***Index Terms*—Monolithic integration, photonic crystal, nanolasers, quantum dots, silicon photonics.**

I. Introduction

The development of data transmission speed through electronic components has been reaching a bottleneck due to the limited bandwidth and power density, despite new nanofabrication method for advanced microprocessor developed with enormous amount of investment. Accordingly, a new technology with advanced Si nanophotonics has been emerged as a promising candidate not only for the next-generation chip-scale data communication network within data centers, but also for the optical computing which has a higher bandwidth, faster speed, and higher power density than the conventional electronic microprocessor [1-3]. To realize a highly efficient, inter/intra-chip communication on Si platform, a new type of Si-based light-emitting source with ultra-small footprint and ultra-low energy consumption is compulsory.

Recently, monolithic integration of III-V optoelectronic devices on Si platform has fueled impressive developments due to its potential in energy-efficient, low-cost and wafer-scale photonic integrated circuits (PICs), even though wafer bonding technology has been extensively investigated [4]. However, material dissimilarities between III-V materials and Si including large mismatch in lattice constant, thermal expansion coefficients, as well as polarity, significantly degrade the crystal quality of metamorphic III-V layers on Si [5, 6], which result in the degraded device performance. Tremendous research efforts have been made through the optimization of sophisticated epitaxial technologies to realize high-quality epitaxial III-V materials with low defect density on complementary metal-oxide-semiconductor (CMOS)-compatible Si or SOI platforms [7-11]. In addition, using III-V quantum dots (QDs) as gain materials for lasers provides various advantages, including insensitivity to defects, low lasing threshold and long lifetime [7, 12]. Owing to the decreased non-radiative recombination ratio, implementing defect-insensitive and high-quality QDs as gain material is regarded as the best solution for highly efficient light-emitting source monolithically grown on Si substrate [13].

Despite considerable research efforts devoted to improving the performance of conventional laser diodes (e.g., ridge-waveguide lasers) grown on Si substrate [13-16], the

Manuscript received July 18, 2021. This work was supported by National Natural Science Foundation of China (No. 62174144), International Cooperation Project (No. 2019A050510002), Shenzhen Key Laboratory Project (No. ZDSYS201603311644527), Shenzhen Fundamental Research Fund (No. JCYJ20150929170644623, No. JCYJ20210324115605016, No. JCYJ20210324120204011), Longgang Key Laboratory Project (No. ZSYS2017003 and No. LGKCZSYS2018000015), Longgang Matching Support Fund (No. CXPTPT-2017-YJ-002 and No. 201617486), Optical Communication Core Chip Research Platform, UK Engineering and Physical Sciences Research Council (EP/P006973/1, EP/T028475/1), National Epitaxy Facility, European project H2020-ICT-PICTURE (780930), Royal Academy of Engineering (RF201617/16/28), French government managed by ANR under the Investissements d'avenir ANR-10-IRT-05 and ANR-15-IDEX-02, French RENATECH network. T Zhou and M. Tang contributed equally to this work.

T. Zhou, M. Tang, J. Park, S. Chen and H. Liu are with the Department of Electronic and Electrical Engineering, University College London, London, Torrington Place, WC1E 7JE, UK (e-mail: mingchu.tang.11@ucl.ac.uk; siming.chen@ucl.ac.uk; huiyun.liu@ucl.ac.uk).

T. Zhou, H. Li, Z, Zhang, Y. Cui and Z. Y. Zhang are with the School of Science and Engineering and Shenzhen Key Lab of Semiconductor Lasers, The Chinese University of Hong Kong, Shenzhen, Guangdong, 518172, P.R. China (email: zhangzy@cuhk.edu.cn).

M. Martin and T. Baron are with Univ. Grenoble Alpes, CNRS, CEA-LETI, MINATEC, Grenoble INP, LTM, F-38054 Grenoble, France.

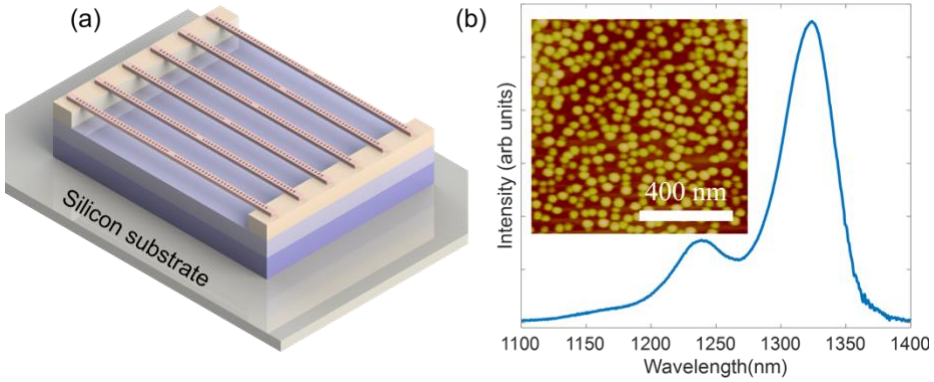

Fig. 1. (a) Schematic diagram of fabricated InAs/GaAs QD PhC nanobeam laser array epitaxially grown on silicon substrate. (b) PL spectra of the as-grown QD gain materials collected at room temperature. The inset shows an AFM image of uncapped InAs/GaAs QDs grown on Si (001) substrate.

integration of nanoscale lasers on CMOS-compatible Si platforms is still the long-standing goals, which is aiming at densely integrated and more energy-efficient Si-based PICs [17]. Until now, microscale lasers, such as microdisk or microring lasers based on whispering gallery mode [11, 18-20], nano-ridge lasers based on Fabry-Pérot cavity [9, 21], and distributed feedback lasers directly grown on Si have been developed [22]. All these efforts contributed to laser miniaturization with a range of improvements including in operating temperature and reduction in lasing threshold. In contrast, using photonic crystal (PhC) to construct nanoscale lasers with diffraction-limited modal volume, can provide highly integrated light sources on Si [23, 24]. Moreover, benefiting from its unique properties such as ultra-high quality (Q)-factor and enhanced light-matter interaction, ultra-compact PhC lasers enable promising advantages such as single-mode lasing operation, thresholdless lasing features and high-speed modulation rates [24-28]. Particularly, the simple and robust one-dimensional (1D) waveguide nature of PhC nanobeam lasers enables a straightforward integration method with other photonic devices [29]. Recently, we presented high performance two-dimensional (2D) QD PhC membrane lasers monolithically grown on CMOS-compatible Si substrate with a low lasing threshold [24], while the physical size of 2D PhC membrane lasers is ~ 20 μm × 20 μm. In this regard, monolithically integrated nanolasers with more compact size are expected to further increase the integration density, as well as to decrease the lasing threshold.

In this work, we report single-mode, room temperature continuous-wave (CW) optically pumped 1D PhC nanobeam lasers monolithically grown on planar CMOS-compatible Si (001) substrate, of which the footprint approaches as small as ~ $8 \times 0.53 \times 0.36$ μm^3 (~ 25 $(\lambda n^{-1})^3$). A tapered air-hole PhC cavity was implemented to achieve a single high Q-factor resonant mode locating within the ground state emission region of as-grown gain material. Single-mode lasing operation with a low lasing threshold of ~ 0.8 μW was obtained for the ultra-compact InAs/GaAs QD PhC nanobeam laser. The ultra-low threshold of PhC nanobeam lasers directly grown on CMOS-compatible Si is comparable with their counterparts on native substrates. The lasing wavelength was also finely tuned over the entire ground state emission region by regularly modifying the structural parameters of devices. The demonstrated Si-based 1D PhC nanobeam lasers with ultra-small footprint, ultra-low energy consumption and waveguide nature of configuration show their advanced potential towards completely integrated light sources on silicon platform.

II. Material Epitaxial Growth and Device Fabrication

The InAs/GaAs QD PhC nanobeam lasers are epitaxially grown on a CMOS-compatible on-axis Si (001) substrate, as shown in Fig. 1(a). A 300 mm diameter Si (001) substrate with a 0.15° misorientation in the [110] direction was pre-treated under high temperature annealing (900 ℃) and hydrogen pressure inside the metal organic chemical vapor deposition system. A 400 nm of GaAs layer was grown as two steps in order to suppress the formation of antiphase boundaries [30]. The GaAs/Si wafer is then diced into 2-inch wafers for molecular beam epitaxy (MBE) growth. A 200 nm GaAs buffer layer was regrown in MBE chamber which attributes to a smooth surface examined by a clear reflective high energy electron diffraction pattern. In order to reduce the non-radiative recombination centers caused by high density of threading dislocations due to the large lattice mismatch between GaAs and Si, four sets of defect filter layers (DFLs) were grown, in which each set of DFLs includes five repeats of $In_{0.18}Ga_{0.82}As$/GaAs strain-layer superlattices grown at 480 ℃ and a 300 nm GaAs spacing layer grown at 590 ℃ [31]. A high temperature in-situ annealing to the strained-layer superlattices were carried out at 590 ℃ for 10 minutes. A 1 μm $Al_{0.6}Ga_{0.4}As$ sacrificial layer was grown on the top of

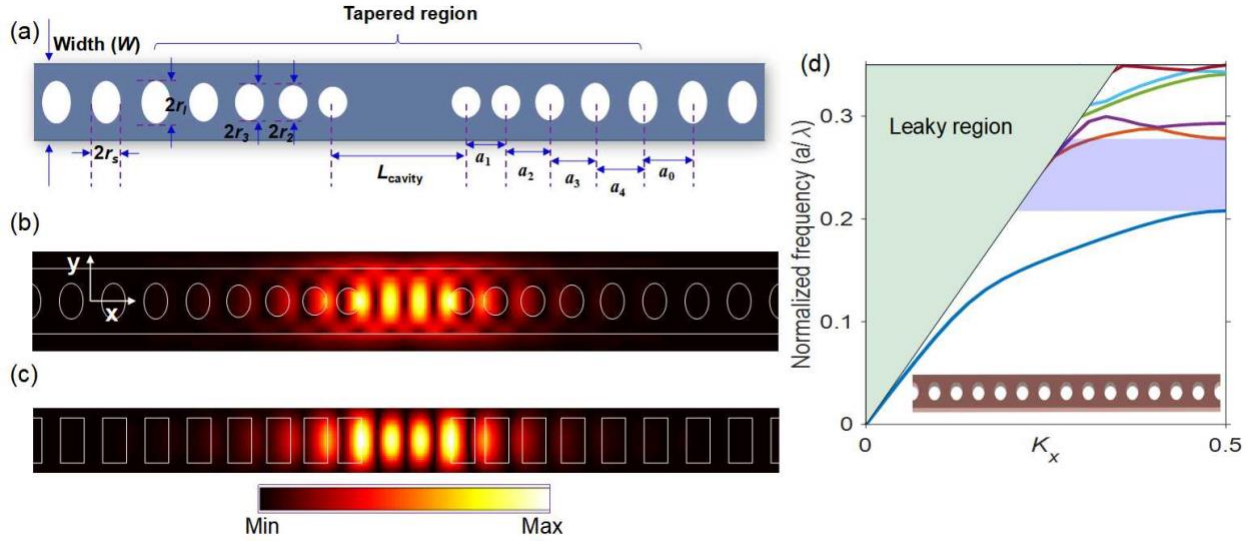

Fig. 2. (a) Top-view schematic of the fabricated InAs/GaAs QD 1D PhC tapered nanobeam cavity comprised of elliptical air-holes. (b) and (c) present the top-view and cross-section view of the calculated E-field profiles for the high *Q*-factor lasing defect mode, calculated by using 3D-FDTD method. The white line represents the boundary of the PhC nanobeam pattern. (d) TE-like states energy band diagram of the 1D PhC nanobeam structure consisted of periodic elliptical air-holes as depicted in the inset. The structural parameters are W = 524 nm, a_0 = 340 nm, r_s/a_0 = 0.27, r_l/r_s = 1.5. The shaded green region is the light cone. The violet region indicates the local photonic band gap.

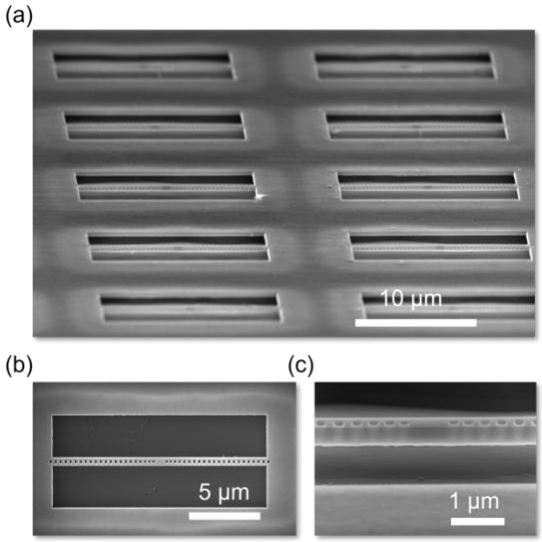

Fig. 3. SEM images of fabricated QD PhC nanobeam laser array (a) and a single nanobeam laser (b) on silicon. (c) A tilted SEM image of tapered cavity region of fabricated PhC nanobeam laser.

DFLs. Four layers of InAs/GaAs dot-in-well (DWELL) work as active region, which is sandwiched between two thin 40 nm $Al_{0.4}Ga_{0.6}As$ cladding layers grown at 600 ℃. Each layer of DWELL consists of three monolayers of InAs deposited on a 2 nm $In_{0.15}Ga_{0.85}As$ quantum well and capped by a 6 nm $In_{0.15}Ga_{0.85}As$ layer at 510 ℃, which were separated by a 50 nm high temperature grown GaAs spacing layer at 590 ℃ [32].

A room-temperature micro-photoluminescence (μ-PL) measurement of the as-grown wafer structure was carried out and the emission spectrum is presented in Fig. 1(b), which indicates a broad ground-state spontaneous emission at around 1.32 μm with a narrow linewidth of ~ 28 meV in O-band. The inset in Fig. 1(b) shows an atomic force microscope (AFM) image of uncapped InAs/GaAs QDs grown on Si (001). The QDs within the active region monolithically grown on Si substrate present a good uniformity with a density of ~ 4×10^{10} cm^{-2}, and a typical size of 25 nm in diameter and 8 nm in height.

A schematic diagram of the fabricated PhC nanobeam cavity is presented in Fig. 2(a). The λ-scale cavity region is enclosed between two tapered PhC Bragg mirrors consisting of elliptical air-holes [33, 34], in which the primary lattice constant (a_0) and size of air-holes are linearly tapered down towards smaller value in the cavity region. The structural parameters of the free-standing PhC nanobeam cavity are $L_{cavity} = 2.64 \times a_0$, $a_4 = a_0 \times 0.96$, $a_i = a_{i+1} \times 0.96$, $r_{i+1}/a_0 = r_i/a_0 + 0.025$ (i = 1 - 3), r_l/r_s = 1.5 and a thickness of ~ 362 nm. To achieve single-mode lasing operation, the PhC nanobeam cavity was designed by using the three-dimensional finite-difference time-domain (3D-FDTD) method, enabling only a single high *Q*-factor defect mode locating within the ground state emission region of gain materials. Figs. 2(b) and 2(c) depict the top and cross-sectional views of the calculated E-field profiles for the high *Q*-factor resonant defect mode, of which the electromagnetic field is tightly confined by index guiding in *y* and *z* directions and Bragg scattering from the periodic PhC mirror in *x* direction. The photonic band diagram of designed PhC nanobeam structure was calculated by MIT Photonic Bands (MPB) based on the plane-wave expansion (PWE) method [35]. Fig. 2(d) shows a calculated TE-like states band diagram of the periodic PhC nanobeam structure with parameters W = 524 nm, a_0 = 340 nm, r_s/a_0 = 0.27, r_l/r_s = 1.5 and a refractive index (n) of 3.4. The calculated normalized PhC local optical band gap frequency (a_0/λ) extends from 0.208 to 0.278 (from 1223 nm to 1635 nm),

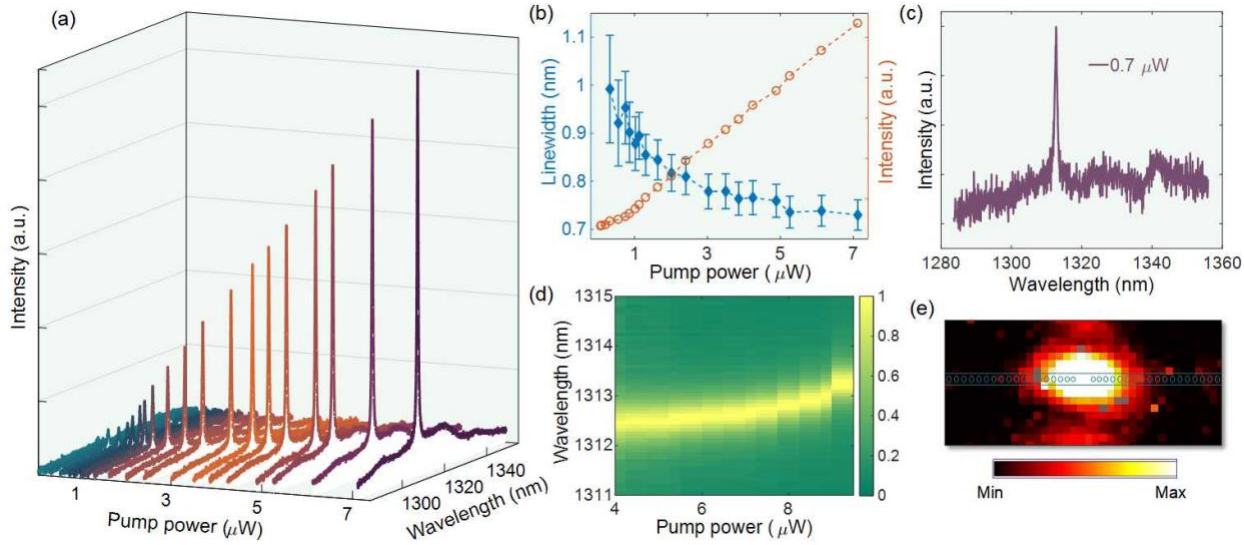

Fig. 4. (a) Power-dependent emission spectra of a PhC nanobeam laser with W = 524 nm, a_0 = 340 nm, r_s/a_0 = 0.27. A sharp lasing peak appears above the spontaneous emission background. a.u., arbitrary units. (b) Collected L-L curve and linewidth of the lasing peak at ~ 1313 nm, indicating a lasing threshold ~ 0.8 μW. (c) Spectra collected just below the threshold. (d) The lasing wavelength under various input pump powers, presenting a redshift of lasing wavelength due to thermal effect. (e) A mode pattern image taken by an infrared camera. The boundary of the PhC nanobeam laser is also indicated in the image. All experiments were carried out at room temperature.

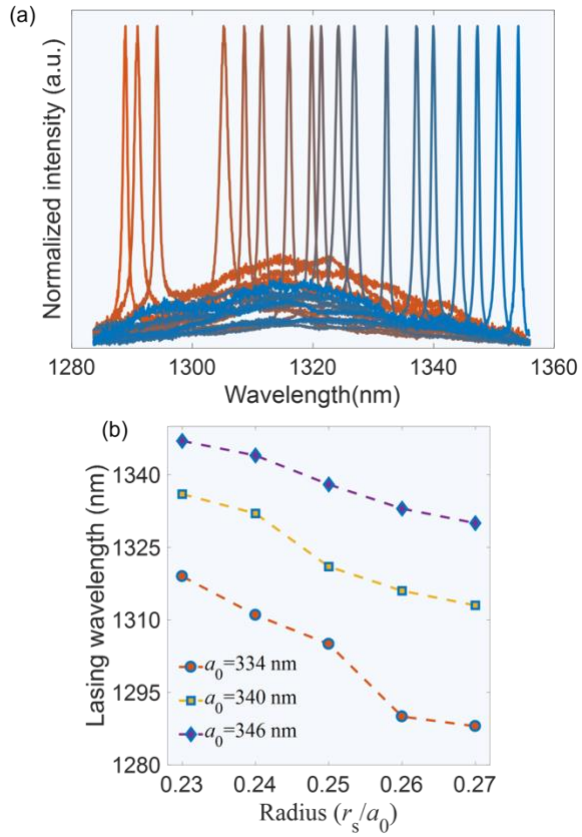

Fig. 5. (a) Normalized measured PL spectra above threshold from representative QD PhC nanobeam lasers with various structural parameters. (b) The lasing wavelength under various radius (r_s/a_0) and lattice constant (a_0) of PhC nanobeam lasers on silicon.

covering the ground-state emission region of as-grown QDs.

The freestanding 1D PhC nanolasers on Si were fabricated by the following nanofabrication processes. A layer of 120 nm silicon dioxide as a hard etching mask was deposited on the as-grown wafer by plasma-enhanced chemical vapor deposition. After the wafer was spin-coated with electron beam resist ZEP-520A, the PhC nanobeam pattern was first defined by using electron beam lithography, and then the pattern was transferred into the hard mask by using plasma etching. Afterwards, the electron beam resist was etched by using O_2 plasma. Then chlorine-based inductively coupled plasma reactive ion etching (ICP-RIE) was implemented to achieve PhC nanobeam structure within gain region. Then, wet etching method was subsequently performed to remove the residual silicon oxide and the sacrificial layer to form a suspended PhC nanobeam.

PhC nanobeam cavity arrays were fabricated by systematically varying the a_0 and r_s of air-holes, resulting in nanolasers with different operating wavelengths. A SEM image of fabricated nanobeam cavity array is depicted in Fig. 3(a), and Fig. 3(b) presents the SEM image of a single PhC nanobeam cavity with a length (x direction) of ~ 15 μm and the width (W) of ~ 524 nm. Vertical and smooth etched air-holes are expected to play a significant role in the performance of PhC nanobeam lasers, especially to minimize the non-radiative surface recombination effect and achieve CW pumped nanolasers operated at room temperature. As presented in Fig. 3(c), a magnified view of cavity region indicates smooth profiles of etched air-holes, which contributes to the low lasing threshold of fabricated devices.

III. NANOLASER OPTICAL MEASUREMENT

The fabricated nanobeam laser were CW optically pumped using a 632.8 nm He-Ne laser as excitation light in a surface-normal μ-PL measurement system. The pumping spot was

focused by a 50× objective with a numerical aperture of 0.42 and was carefully positioned in the PhC nanobeam cavity

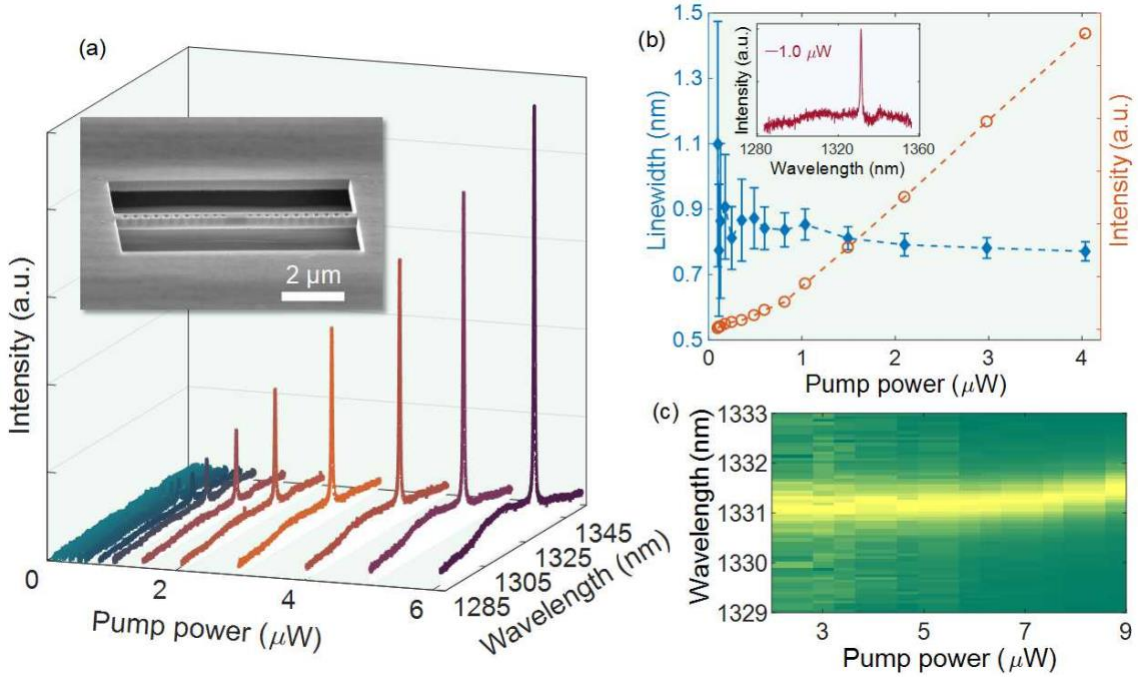

Fig. 6. (a) Power-dependent emission spectra of a more compact single-mode PhC nanobeam laser on silicon. The structural parameters are W = 530 nm, a_0 = 346 nm, r_s/a_0 = 0.26. Inset: A tilted SEM image of the fabricated nanobeam laser. (b) Collected L-L curve and linewidth of the lasing peak at ~ 1331 nm, indicating a lasing threshold ~ 0.9 μW. (c) The lasing wavelength under various input pump powers.

region by using piezo-electric nanopositioners. The diameter of the pump spot size is around 1.2 μm to 2.5 μm under implemented incident pump powers. And the pump powers of the fabricated nanobeam lasers were directly measured by replacing the fabricated devices with a power meter. The output light of PhC nanobeam lasers was collected from the top by using the same objective and analyzed by a monochromator with an InGaAs detector cooled by liquid nitrogen. Single-mode lasing emission was observed for many PhC nanobeam lasers fabricated on the same wafer. Fig. 4(a) depicts measured power-dependent spectra of a single-mode PhC nanobeam laser with structural parameters W = 524 nm, a_0 = 340 nm and r_s/a_0 = 0.27. A sharp lasing peak (~ 1313 nm) is observed above the spontaneous emission background, which is within the ground state emission of QDs. Mainly caused by the fluctuations in fabrication, a slight difference exists between the designed lasing wavelength and measured value, as well as the measured Q-factor ($Q = \lambda/\Delta\lambda$ = 1500) is smaller than the calculated value (~ 4000). The collected L-L (light-out versus light-in) curve and the linewidth of the lasing peak under various pump powers are shown in Fig. 4(b), providing the evidence of the lasing operation with a kink of L–L curve and the spectral linewidth narrowing effect. The measured lasing threshold (P_{th}) is around 0.8 μW driven from the L–L curve, which should be lower if considering the absorption efficiency of excitation light and the effective pump area [36]. The lasing spectra measured just below the threshold with a growing resonant peak from the spontaneous emission background is depicted in Fig. 4(c). The power-dependent measured lasing wavelengths present a clear redshift under increased pump power as displayed in Fig. 4(d), which was mainly induced by the change of the refractive index due to the heating of the cavity. Fig. 4(e) shows a mode pattern image taken above threshold by an infrared camera, indicating a strong light spot in the central cavity region of PhC nanobeam laser.

The feasibility of tunable nanolasers on Si were preliminarily tested by varying the structural parameters of designed PhC nanobeam cavities. As illustrated in Fig. 5(a), a wide range of tunable lasing wavelengths around the ground state region was achieved in the fabricated PhC nanobeam lasers. For nanobeam lasers operating away from the central peak of ground state emission, a relatively intense spontaneous emission background exists in the collected lasing spectra, which is expected to be further suppressed by increasing the layers of QDs and optimizing the etching profiles of devices. The size of air-holes or lattice constant varies slowly across the designed PhC nanobeam array, resulting in a gradual shift in the lasing wavelength. Though there could be slight discrepancies between measured and designed wavelengths owing to the fabrication fluctuations such as the edge roughness of air-holes, the lasing wavelengths show a regular trend under various radius (r_s/a_0) and lattice constant (a_0) as presented in Fig. 5(b). The lasing wavelengths were systematically blue-shifted with increasing the radius of air-holes (or decreasing the lattice constant) due to the decreased effective refractive index. This feature of tunable wavelength may be useful for the future development of ultra-compact dense-wave-division-multiplexing light sources on Si.

To further pursuit compact size of the PhC laser, PhC nanobeam cavity with less air-holes was designed to decrease the size of integrated lasers on Si, even though suffering from a weakened mode confinement. However, the proper choice and design of the numbers of air-holes will not degrade the *Q*-factor critically. Therefore, lasing operation can still be sustained within such a small 1D PhC nanocavity. This kind of compact nanobeam laser with tapered cavity region also has the capability for the future integrated electrically pumped nanolasers on Si [37]. Fig. 6(a) presents power-dependent lasing spectra of a single-mode PhC nanobeam laser with a small physical volume of ~ $8 \times 0.53 \times 0.36\ \mu m^3$ (~ $25\ (\lambda n^{-1})^3$). The inset of Fig. 6(a) shows a tilted SEM image of the fabricated ultra-compact 1D PhC nanobeam laser. The measured output PL intensity and the linewidth of the lasing peak as a function of incident pump powers are shown in Fig. 6(b), which exhibits the evidence of the lasing operation with a threshold estimated ~ 0.9 μW. The inset of Fig. 6(b) shows the measured spectra just above the threshold. A redshift of lasing peak under higher pump power was also observed in this ultra-compact 1D PhC nanobeam laser, as presented in Fig. 6(c). The presented lasing threshold P_{th} of the fabricated 1D PhC nanolasers directly grown on Si is in the same order of PhC lasers grown on its native substrate [38-40], which is mainly attributed to the insensitivity to defects and high crystal quality of the grown QDs on Si. A fabricated high *Q*-factor PhC nanocavity is also essential to achieve the laser operation at room temperature under CW excitation [38].

IV. Conclusion

In conclusion, we report ultra-compact InAs/GaAs QD 1D PhC nanobeam lasers monolithically grown on a planar CMOS-compatible Si (001) substrate. The fabricated PhC nanobeam lasers were CW optically pumped under room temperature, exhibiting a single-mode lasing operation and a low lasing threshold of ~ 0.8 μW. Besides, multi-integrated laser sources were preliminarily studied by slightly tuning the lattice constant or radius of air-holes of a PhC nanobeam laser array. The demonstrated ultra-compact Si-based 1D PhC nanobeam lasers in this work are expected to play a key role in the photonic applications such as short-distance optical communication and data centers.

Acknowledgment

The authors would like to thank Xuexuan Qu, Yao Wang and Rui Zhang from the Core Research Facilities of Southern University of Science and Technology for the technical help in device fabrication.

References

[1] R. Soref, "The past, present, and future of silicon photonics," *IEEE Journal of selected topics in quantum electronics,* vol. 12, no. 6, pp. 1678-1687, 2006.

[2] T. Komljenovic, D. Huang, P. Pintus, M. A. Tran, M. L. Davenport, and J. E. Bowers, "Photonic integrated circuits using heterogeneous integration on silicon," *Proceedings of the IEEE,* vol. 106, no. 12, pp. 2246-2257, 2018.

[3] C. Sun *et al.*, "Single-chip microprocessor that communicates directly using light," *Nature,* vol. 528, no. 7583, pp. 534-538, 2015.

[4] R. Helkey, A. A. Saleh, J. Buckwalter, and J. E. Bowers, "High-performance photonic integrated circuits on silicon," *IEEE Journal of Selected Topics in Quantum Electronics,* vol. 25, no. 5, pp. 1-15, 2019.

[5] Q. Li and K. M. Lau, "Epitaxial growth of highly mismatched III-V materials on (001) silicon for electronics and optoelectronics," *Progress in Crystal Growth and Characterization of Materials,* vol. 63, no. 4, pp. 105-120, 2017.

[6] H. Kroemer, "Polar-on-nonpolar epitaxy," *Journal of Crystal Growth,* vol. 81, no. 1-4, pp. 193-204, 1987.

[7] S. Chen *et al.*, "Electrically pumped continuous-wave III–V quantum dot lasers on silicon," *Nature Photonics,* vol. 10, no. 5, pp. 307-311, 2016.

[8] M. R. Calvo *et al.*, "Mid-infrared laser diodes epitaxially grown on on-axis (001) silicon," *Optica,* vol. 7, no. 4, pp. 263-266, 2020.

[9] Y. Han, Z. Yan, W. K. Ng, Y. Xue, K. S. Wong, and K. M. Lau, "Bufferless 1.5 μm III-V lasers grown on Si-photonics 220 nm silicon-on-insulator platforms," *Optica,* vol. 7, no. 2, pp. 148-153, 2020.

[10] Z.-H. Wang, W.-Q. Wei, Q. Feng, T. Wang, and J.-J. Zhang, "InAs/GaAs quantum dot single-section mode-locked lasers on Si (001) with optical self-injection feedback," *Optics Express,* vol. 29, no. 2, pp. 674-683, 2021/01/18 2021.

[11] W.-Q. Wei *et al.*, "Phosphorus-free 1.5 μm InAs quantum-dot microdisk lasers on metamorphic InGaAs/SOI platform," *Optics letters,* vol. 45, no. 7, pp. 2042-2045, 2020.

[12] J. C. Norman *et al.*, "A review of high-performance quantum dot lasers on silicon," *IEEE Journal of Quantum Electronics,* vol. 55, no. 2, pp. 1-11, 2019.

[13] M. Tang *et al.*, "Integration of III-V lasers on Si for Si photonics," *Progress in Quantum Electronics,* vol. 66, pp. 1-18, 2019.

[14] J. Kwoen, B. Jang, K. Watanabe, and Y. Arakawa, "High-temperature continuous-wave operation of directly grown InAs/GaAs quantum dot lasers on on-axis Si (001)," *Optics express,* vol. 27, no. 3, pp. 2681-2688, 2019.

[15] S. Liu *et al.*, "High-channel-count 20 GHz passively mode-locked quantum dot laser directly grown on Si with 4.1 Tbit/s transmission capacity," *Optica,* vol. 6, no. 2, pp. 128-134, 2019.

[16] J. Kwoen, B. Jang, J. Lee, T. Kageyama, K. Watanabe, and Y. Arakawa, "All MBE grown InAs/GaAs quantum dot lasers on on-axis Si (001)," *Optics express,* vol. 26, no. 9, pp. 11568-11576, 2018.

[17] M. T. Hill and M. C. Gather, "Advances in small lasers," *Nature Photonics,* vol. 8, no. 12, pp. 908-918, 2014.

[18] Y. Wan *et al.*, "Low-threshold continuous-wave operation of electrically pumped 1.55 μm InAs quantum dash microring lasers," *ACS Photonics,* vol. 6, no. 2, pp. 279-285, 2018.

[19] T. Zhou *et al.*, "Ultra-low threshold InAs/GaAs quantum dot microdisk lasers on planar on-axis Si (001) substrates," *Optica,* vol. 6, no. 4, pp. 430-435, 2019/04/20 2019.

[20] S. Zhu, B. Shi, and K. M. Lau, "Electrically pumped 1.5 μm InP-based quantum dot microring lasers directly grown on (001) Si," *Optics letters,* vol. 44, no. 18, pp. 4566-4569, 2019.

[21] Y. Han, W. K. Ng, Y. Xue, Q. Li, K. S. Wong, and K. M. Lau, "Telecom InP/InGaAs nanolaser array directly grown on (001) silicon-on-insulator," *Optics letters,* vol. 44, no. 4, pp. 767-770, 2019.

[22] Z. Wang *et al.*, "Room-temperature InP distributed feedback laser array directly grown on silicon," *Nature Photonics,* vol. 9, no. 12, pp. 837-842, 2015.

[23] S. Mauthe *et al.*, "Hybrid III–V Silicon Photonic Crystal Cavity Emitting at Telecom Wavelengths," *Nano Letters,* vol. 20, no. 12, pp. 8768-8772, 2020.

[24] T. Zhou *et al.*, "Continuous-wave quantum dot photonic crystal lasers grown on on-axis Si (001)," *Nature Communications,* vol. 11, no. 1, p. 977, 2020/02/20 2020.

[25] Y. Akahane, T. Asano, B.-S. Song, and S. Noda, "High-Q photonic nanocavity in a two-dimensional photonic crystal," *Nature,* vol. 425, no. 6961, pp. 944-947, 2003/10/01 2003.

[26] S. Matsuo *et al.*, "High-speed ultracompact buried heterostructure photonic-crystal laser with 13 fJ of energy consumed per bit

transmitted," *Nature Photonics,* vol. 4, no. 9, pp. 648-654, 2010/09/01 2010.

[27] B. Ellis *et al.*, "Ultralow-threshold electrically pumped quantum-dot photonic-crystal nanocavity laser," *Nature Photonics,* vol. 5, no. 5, pp. 297-300, 2011/05/01 2011.

[28] I. Prieto *et al.*, "Near thresholdless laser operation at room temperature," *Optica,* vol. 2, no. 1, pp. 66-69, 2015/01/20 2015.

[29] Y. Halioua *et al.*, "Hybrid III-V semiconductor/silicon nanolaser," *Optics Express,* vol. 19, no. 10, pp. 9221-9231, 2011/05/09 2011.

[30] R. Alcotte *et al.*, "Epitaxial growth of antiphase boundary free GaAs layer on 300 mm Si(001) substrate by metalorganic chemical vapour deposition with high mobility," *APL Materials,* vol. 4, no. 4, p. 046101, 2016.

[31] M. Tang *et al.*, "Optimizations of Defect Filter Layers for 1.3-μm InAs/GaAs Quantum-Dot Lasers Monolithically Grown on Si Substrates," *IEEE Journal of Selected Topics in Quantum Electronics,* vol. 22, no. 6, pp. 50-56, 2016.

[32] H. Y. Liu *et al.*, "Improved performance of 1.3μm multilayer InAs quantum-dot lasers using a high-growth-temperature GaAs spacer layer," *Applied Physics Letters,* vol. 85, no. 5, pp. 704-706, 2004.

[33] P. B. Deotare, M. W. McCutcheon, I. W. Frank, M. Khan, and M. Lončar, "High quality factor photonic crystal nanobeam cavities," *Applied Physics Letters,* vol. 94, no. 12, p. 121106, 2009.

[34] T.-W. Lu, L.-H. Chiu, P.-T. Lin, and P.-T. Lee, "One-dimensional photonic crystal nanobeam lasers on a flexible substrate," *Applied Physics Letters,* vol. 99, no. 7, p. 071101, 2011.

[35] S. G. Johnson and J. D. Joannopoulos, "Block-iterative frequency-domain methods for Maxwell's equations in a planewave basis," *Optics express,* vol. 8, no. 3, pp. 173-190, 2001.

[36] T. Zhou *et al.*, "Microscale local strain gauges based on visible micro-disk lasers embedded in a flexible substrate," *Optics Express,* vol. 26, no. 13, pp. 16797-16804, 2018/06/25 2018.

[37] K.-Y. Jeong *et al.*, "Electrically driven nanobeam laser," *Nature communications,* vol. 4, no. 1, pp. 1-6, 2013.

[38] M. Nomura *et al.*, "Room temperature continuous-wave lasing in photonic crystal nanocavity," *Optics Express,* vol. 14, no. 13, pp. 6308-6315, 2006.

[39] K. Tanabe, M. Nomura, D. Guimard, S. Iwamoto, and Y. Arakawa, "Room temperature continuous wave operation of InAs/GaAs quantum dot photonic crystal nanocavity laser on silicon substrate," *Optics Express,* vol. 17, no. 9, pp. 7036-7042, 2009/04/27 2009.

[40] Y. Gong, B. Ellis, G. Shambat, T. Sarmiento, J. S. Harris, and J. Vučković, "Nanobeam photonic crystal cavity quantum dot laser," *Optics express,* vol. 18, no. 9, pp. 8781-8789, 2010.